# A Correlation-Based Stochastic Model for Massive MIMO Channel

**Yang Liu[1], Gang Li[2], Chengxiang Wang[1,3,*]**

[1] National Mobile Communications Research Laboratory, School of Information Science and Engineering, Southeast University, Nanjing 211189, China

[2] School of Internet of Things Engineering, Jiangnan University, Wuxi 214122, China

[3] Pervasive Communication Research Center, Purple Mountain Laboratories, Nanjing 211111, China

[*] The corresponding author, email: chxwang@seu.edu.cn

**Cite as:** Y. Liu, G. Li, *et al*., "A correlation-based stochastic model for massive mimo channel," *China Communications*, 2024, vol. 21, no. 1, pp. 175-187. **DOI**: 10.23919/JCC.ja.2022-0739

**Abstract:** In this paper, the channel impulse response matrix (CIRM) can be expressed as a sum of couplings between the steering vectors at the base station (BS) and the eigenbases at the mobile station (MS). Nakagami distribution was used to describe the fading of the coupling between the steering vectors and the eigenbases. Extensive measurements were carried out to evaluate the performance of this proposed model. Furthermore, the physical implications of this model were illustrated and the capacities are analyzed. In addition, the azimuthal power spectrum(APS) of several models was analyzed. Finally, the channel hardening effect was simulated and discussed. Results showed that the proposed model provides a better fit to the measured results than the other CBSM, i.e., Weichselberger model. Moreover, the proposed model can provide better tradeoff between accuracy and complexity in channel synthesis. This CIRM model can be used for massive MIMO design in the future communication system design.

**Keywords:** CBSM; channel capacity; channel hardening; channel modeling; massive MIMO

**Received:** Oct. 12, 2022
**Revised:** Jun. 02, 2023
**Editor:** Linglong Dai

## I. INTRODUCTION

The sixth generation (6G) wireless communication system has gotten a lot of attention since the previous system could not meet all demands of the future around 2030 [1, 2]. Compared with the previous communication network, 6G has been expected to provide a much higher data rate (Tbps), lower latency, and wider coverage [3, 4]. Massive multiple input multiple output (MIMO) has been seen as one of the promising air interface technologies to achieve high performance metrics [5, 6]. As an enhanced MIMO technology, massive MIMO may exploit hundreds or thousands antennas in the communication system to improve spectral efficiency, reliability, and throughputs [7]. This technology can be used in lots of ultra-reliable and low latency communication scenarios such as Industrial Internet of Things (IIoT), unmanned system, and high speed train (HST) network [8, 9]. Accurate and efficient channel models are very important to design, evaluate and optimize the massive MIMO wireless communication system [10, 11].

Studies on MIMO channel could trace back to the 1980s [12]. In theory, modeling MIMO channel included deterministic and stochastic [13, 14]. Deterministic method, such as ray tracing, needs detailed descriptions of the environment and its computational complexity is very high. On the contrary, stochastic

methods are much more flexible and have been intensively studied in the past decades [15–17]. Generally, studies on stochastic models could be categorized into roughly three types. The first type is geometrical based stochastic model (GBSM) [18, 19]. In this model, the scatterers in the propagation environment are assumed to possess some geometric statistical distributions. Then, the channel impulse response (CIR) could be obtained by the simple ray tracing modeling. Many standardized models, i.e., IMT-2020 [20], 3GPP [21], COST-2100 [22], and QuaDRiGa [23], are attached to the kind of GBSM. The second type is parametric-based stochastic model (PBSM). The statistical properties of channel parameters, such as amplitude, delay, and angle of arrival (AoA) or departure (AoD) are revealed to generate the PBSM [24–26]. The third approach is correlation-based stochastic model (CBSM) [27–29]. These models generate the CIR matrices according to mutual correlations of propagation channel. Compared with the other two types of models, CBSM aims to describe spatial multiplexing, diversity, and beamforming properties of MIMO channel. Most of the current standardized models are based on GBSM. However, with the continuous increase of massive MIMO antenna arrays, the advantages of CBSM are constantly emerging, and it is expected to be widely used in the future [29].

Typical CBSMs include Kronecker model [27], virtual channel representation (VCR) [28], and Weichselberger model [29]. The Kronecker model assumes that the transmitter (Tx) and receiver (Rx) are independent. Thus, the full correlation matrix could be decomposed into the Kronecker product of the single-sided correlation matrix at the Tx and Rx. VCR takes into account the mutual dependency of the correlations at both ends. Using the coupling matrix to model the mutual dependency of both link sides. Then the channel impulse response matrix (CIRM) could be expressed as a sum of the couplings between the predefined steering vectors at Tx and Rx sides. Combine the advantages of Kronecker and VCR, Weichselberger model utilizes the eigenbases instead of predefined steering vectors to represent the correlations of each side. The eigenbases are defined as the eigenvectors of the single-sided correlation matrix. Thus, the CIRM could be modeled as a sum of the couplings between the eigenbases at the Tx and Rx ends.

Basically, Weichselberger model describes the properties of the MIMO channel most accurately in the above three models. However, when it comes to massive MIMO, the complexity of Weibchselberger model would be quite high as the increasing number of antennas. How to provide a tradeoff between accuracy and complexity would be a challenging task. Moreover, all the above three CBSMs use Rayleigh distribution to model the coupling matrix. But several measurement results have shown that Rayleigh distribution is inapplicable to the fading properties in the rich scattering environments [30, 31]. A CBSM that could reveal the small scale fading accurately would be more accurate. Finally, massive MIMO can effectively reduce the mutual interference among multiple users, as known as the channel hardening effect some literatures have shown [32–34]. However, this effect in the different propagation environments needs further study. An accurate CBSM would be suitable for analyzing channel hardening effect in the various scattering environments.

To the best of our knowledge, a general CBSM that provides a tradeoff between accuracy and complexity and describes the small scale fading accurately is still missing. Furthermore, based on the general CBSM, we can study the capacity properties and reveal the channel hardening effect in various channels. Considering the existing research gaps, a general CBSM for the massive MIMO channel in 6G communication system is proposed in this paper. The contributions of this paper are listed as follows:

1. A novel massive MIMO model is proposed. The CIRM is expressed as a sum of couplings between the steering vectors at base station (BS) side and eigenbases at mobile station (MS) side.

2. The accuracy of the Nakagami distribution in describing the fading properties is proved.

3. Through the comparison of channel capacity, azimuthal power spectrum(APS), the difference between the proposed model and existing models is illustrated. It shows the advantages of the proposed model, that is, it provides a tradeoff between accuracy and complexity in the field of massive MIMO channel modeling.

The rest of the paper is organized as follows. In Section II, a novel CIRM model for massive MIMO channel is proposed. Section III describes the setups of massive MIMO channel measurements. Section IV analyzes the complexity and accuracy of the proposed model. In Section IV, five sample coupling matrices

and their corresponding channel characteristics are introduced. The influence of the number of receiving antennas ($N_{\mathrm{MS}}$) and the number of transmitting antennas ($N_{\mathrm{BS}}$) on channel characteristics is analyzed from two aspects of channel capacity and channel hardening. Section V, conclusions of the main innovation points and experimental results are summarized.

## II. CHANNEL MODEL AND PARAMETER EXTRACTION

### 2.1 Massive MIMO Channel Model

The proposed model is based on the following assumptions.

Assumption 1: the eigenbases of the single-sided correlation matrix are only determined by the propagation environment, and do not vary with spatial covariance matrix.

Assumption 2: the eigenbases of the single-sided correlation matrix must be the steering matrices at the BS side.

Assumption 3: the fading process between BS and MS possesses the Nakagami distribution.

Firstly, the spatial characteristics of a general MIMO channel can be presented by a generic full correlation matrix [29]. This matrix can be represented as

$$\boldsymbol{R}_{\boldsymbol{H}} = \mathrm{E}_{\boldsymbol{H}}(\mathrm{vec}(\boldsymbol{H}) \cdot \mathrm{vec}(\boldsymbol{H})^{\mathrm{H}}), \tag{1}$$

where vec $(\cdot)$ represents the combination of all the column vectors in the matrix into a column vector, and $(\cdot)^{\mathrm{H}}$ represents the conjugate transpose matrix of the matrix.

Similarly, the spatial characteristics of the BS or MS can be represented by a single-sided correlation matrix, which can be expressed as

$$\boldsymbol{R}_{\mathrm{MS},\boldsymbol{Q}_{\mathrm{BS}}} = \mathrm{E}_{\boldsymbol{H}}(\boldsymbol{H}\boldsymbol{Q}_{\mathrm{BS}}\boldsymbol{H}^{\mathrm{H}}), \tag{2}$$

and

$$\boldsymbol{R}_{\mathrm{BS},\boldsymbol{Q}_{\mathrm{MS}}} = \mathrm{E}_{\boldsymbol{H}}(\boldsymbol{H}\boldsymbol{Q}_{\mathrm{MS}}\boldsymbol{H}^{\mathrm{H}}), \tag{3}$$

where $\boldsymbol{Q}_{\mathrm{BS}}$ and $\boldsymbol{Q}_{\mathrm{MS}}$ represent the spatial correlation matrix of BS side and MS side respectively.

According to assumption 1

$$\boldsymbol{R}_{\mathrm{MS},\boldsymbol{Q}_{\mathrm{BS}}} = \boldsymbol{U}_{\mathrm{MS}}\boldsymbol{\Lambda}_{\mathrm{MS},\boldsymbol{Q}_{\mathrm{BS}}}\boldsymbol{U}_{\mathrm{MS}}^{\mathrm{H}}, \tag{4}$$

and

$$\boldsymbol{R}_{\mathrm{BS},\boldsymbol{Q}_{\mathrm{MS}}} = \boldsymbol{U}_{\mathrm{BS}}\boldsymbol{\Lambda}_{\mathrm{BS},\boldsymbol{Q}_{\mathrm{MS}}}\boldsymbol{U}_{\mathrm{BS}}^{\mathrm{H}}, \tag{5}$$

where $\boldsymbol{U}_{\mathrm{BS}}$ and $\boldsymbol{U}_{\mathrm{MS}}$ represent the single-sided correlation matrix of the BS (MS) side, which does not change with the spatial covariance matrix.

According to assumption 2

$$\boldsymbol{U}_{\mathrm{BS}}=\boldsymbol{A}_{\mathrm{BS}}, \tag{6}$$

$$\boldsymbol{A}_{\mathrm{BS}} = (\boldsymbol{a}_{BS}^{1}, \cdots, \boldsymbol{a}_{\mathrm{BS}}^{N_{\mathrm{BS}}}), \tag{7}$$

$$\boldsymbol{a}_{\mathrm{BS}}^{j} = (1, e^{-i2\pi\alpha_j}, \cdots, e^{-i2\pi(N-1)\boldsymbol{\alpha}_j}), \tag{8}$$

and

$$\boldsymbol{\alpha}_j = d\sin(j \times 2\pi/N_{\mathrm{BS}})/\lambda, \tag{9}$$

where $\boldsymbol{A}_{\mathrm{BS}}$ is the steering matrices of BS, $\boldsymbol{a}_{\mathrm{BS}}^{j}$( $j$=1,⋯,$N_{\mathrm{BS}}$ ) are the steering vectors at BS. The matrix composed of these steering vectors is the steering matrix at MS side. The variable $d$ represents the antenna space, $\lambda$ is wavelength.

According to assumption 3, with the increase of array size, the eigenbases at MS side and steering vectors at BS side may experience different scatters. Therefore, Nakagami distribution may give much accurate description of the fading process than Rayleigh distribution since Nakagami distribution is an extension of Rayleigh distribution and has already proved to be more useful than Rayleigh distribution.

Calculate the single-sided correction matrix at MS and BS side as

$$\begin{aligned}\boldsymbol{R}_{\mathrm{MS},\boldsymbol{Q}_{\mathrm{BS}}} &= \mathrm{E}_{\boldsymbol{H}}(\boldsymbol{H}\boldsymbol{Q}_{\mathrm{BS}}\boldsymbol{H}^{\mathrm{H}}) \\ &= \boldsymbol{U}_{\mathrm{MS}}\boldsymbol{\Lambda}_{\mathrm{MS}}\boldsymbol{H}_{\mathrm{MS}}^{\mathrm{H}},\end{aligned} \tag{10}$$

$$\boldsymbol{\Lambda}_{\mathrm{MS}} = \mathrm{E}_{\boldsymbol{H}}\left((\mathbf{O} \odot e^{i\boldsymbol{\Theta}})\boldsymbol{A}_{\mathrm{BS}}^{\mathrm{T}}\boldsymbol{Q}_{\mathrm{BS}}\boldsymbol{A}_{\mathrm{BS}}^{*}(\boldsymbol{O} \odot \mathrm{e}^{\mathrm{i}\boldsymbol{\Theta}})^{\mathrm{H}}\right), \tag{11}$$

$$\begin{aligned}\boldsymbol{R}_{\mathrm{BS},\boldsymbol{Q}_{\mathrm{MS}}} &= \mathrm{E}_{\boldsymbol{H}}(\boldsymbol{H}\boldsymbol{Q}_{\mathrm{MS}}\boldsymbol{H}^{\mathrm{H}}) \\ &= \boldsymbol{U}_{\mathrm{BS}}\boldsymbol{\Lambda}_{\mathrm{BS}}\boldsymbol{H}_{\mathrm{BS}}^{\mathrm{H}},\end{aligned} \tag{12}$$

and

$$\boldsymbol{\Lambda}_{\mathrm{BS}} = \mathrm{E}_{\boldsymbol{H}}\left((\boldsymbol{O} \odot e^{i\boldsymbol{\Theta}})\boldsymbol{A}_{\mathrm{MS}}^{\mathrm{T}}\boldsymbol{Q}_{\mathrm{MS}}\boldsymbol{A}_{MS}^{*}(\boldsymbol{O} \odot e^{i\boldsymbol{\Theta}})^{\mathrm{H}}\right). \tag{13}$$

In addition, the uniformly distributed i.i.d. entries of $\boldsymbol{\Theta}$ give

$$E(e^{i[\boldsymbol{\Theta}]_{mn}}e^{i[\boldsymbol{\Theta}]_{jk}}) = \begin{cases} 1, & m = j, n = k \\ 0, & else \end{cases}. \tag{14}$$

According to which can express the elements of the matrices $\boldsymbol{\Theta}_{\mathrm{BS}}$ and $\boldsymbol{\Theta}_{\mathrm{MS}}$ as

$$\begin{aligned}[\boldsymbol{\Lambda}_{\mathrm{MS}}]_{jk} &= \sum_{l'=1}^{N_{\mathrm{MS}}}\sum_{l=1}^{N_{\mathrm{MS}}}[\boldsymbol{O}]_{jl}e^{i[\boldsymbol{\Theta}]_{jl}}[\boldsymbol{Q'}_{\mathrm{MS}}]_{ll'}[\boldsymbol{O}]_{kl'}e^{-i[\boldsymbol{\Theta}]_{kl'}} \\ &= \begin{cases} \sum\limits_{l=1}^{N_{\mathrm{MS}}}[\boldsymbol{Q'}_{\mathrm{MS}}]_{ll}[\boldsymbol{O}]_{lj}^{2}, & j = k \\ 0, & j \neq k \end{cases},\end{aligned} \tag{15}$$

and

$$\begin{aligned}[\boldsymbol{\Lambda}_{\mathrm{BS}}]_{jk} &= \sum_{l'=1}^{N_{\mathrm{BS}}}\sum_{l=1}^{N_{\mathrm{BS}}}[\boldsymbol{O}]_{jl}e^{i[\boldsymbol{\Theta}]_{jl}}[\boldsymbol{Q'}_{\mathrm{BS}}]_{ll'}[\boldsymbol{O}]_{kl'}e^{-i[\boldsymbol{\Theta}]_{kl'}} \\ &= \begin{cases} \sum\limits_{l=1}^{N_{\mathrm{BS}}}[\boldsymbol{Q'}_{\mathrm{BS}}]_{ll}[\boldsymbol{O}]_{lj}^{2}, & j = k \\ 0, & j \neq k \end{cases},\end{aligned} \tag{16}$$

where $\boldsymbol{A}_{\mathrm{BS}}^{\mathrm{T}}\boldsymbol{Q}_{\mathrm{BS}}\boldsymbol{Q}_{\mathrm{BS}}^{*} = \boldsymbol{Q}'_{\mathrm{BS}}$, $\boldsymbol{A}_{\mathrm{MS}}^{\mathrm{T}}\boldsymbol{Q}_{\mathrm{MS}}\boldsymbol{Q}_{\mathrm{MS}}^{*} = \boldsymbol{Q}'_{\mathrm{MS}}$. Thus, $\boldsymbol{\Theta}_{\mathrm{BS}}$ and $\boldsymbol{\Theta}_{\mathrm{MS}}$ are diagonal matrices.

According to equation (1)–(16), MIMO channel can be modeled by (17) when these three assumptions stand:

$$\boldsymbol{H} = \boldsymbol{U}_{\mathrm{MS}}(\boldsymbol{O} \odot \mathrm{e}^{i\boldsymbol{\Theta}})\boldsymbol{A}_{\mathrm{BS}}^{\mathrm{T}}, \tag{17}$$

where $\boldsymbol{U}_{\mathrm{MS}}$ is a unitary matrix. The entries of the matrix $\boldsymbol{O}$ are independent identical Nakagami distributed variables. The entry $[\boldsymbol{O}]_{jk}$ represents the amplitude gain of the virtual link between the *j*th steering vector at BS side and the *k*th eigenbasis at MS side. And $\odot$ represents multiplying corresponding elements. The symbol *i* represents imaginary unit. The entries of the matrix $\boldsymbol{\Theta}$ are independent identical uniform distributed variables among [0,2$\pi$]. See (7)–(10) for detailed informations of $\boldsymbol{A}_{\mathrm{BS}}$.

## 2.2 Model Parameters Extraction

The parameters to be extracted are the eigenbases of MS side and the entries of Nakagami distribution in the random matrix $\boldsymbol{O}$.

The eigenbases at MS side can be obtained by eigendecomposition of the unparameterized single-sided correlation matrix and expressed by:

$$\begin{aligned}\boldsymbol{R}_{\mathrm{MS}} &= \mathrm{E}_{\boldsymbol{H}}(\boldsymbol{H}^{\mathrm{H}}\boldsymbol{H}) \\ &= \boldsymbol{U}_{\mathrm{MS}}\left(\sum_{i=1}^{N_{\mathrm{BS}}}\mathrm{diag}(\lambda_{i0})\right)\boldsymbol{U}_{\mathrm{MS}}^{\mathrm{H}},\end{aligned} \tag{18}$$

where diag $(\cdot)$ means to place the elements of a column vector at the main diagonal positions of a square matrix. And $\lambda_{i0}$ is the eigenvalue of the single-sided correlation matrix at BS side.

The random elements in the matrix follow Nakagami distribution, whose parameters can be calculated by:

$$m_{jk} = \mathrm{E}_{\mathbf{H}}^{2}(\left\|(\boldsymbol{a}_{\mathrm{BS}}^{j})^{\mathrm{H}}\mathbf{H}\mathbf{u}_{k}\right\|^{2})/\mathrm{var}(\left\|(\boldsymbol{a}_{\mathrm{BS}}^{j})^{\mathrm{H}}\mathbf{H}\mathbf{u}_{k},\right\|^{2}), \tag{19}$$

$$\Omega_{jk} = \mathrm{E}_{\boldsymbol{H}}^{2}(\left\|(\boldsymbol{a}_{\mathrm{BS}}^{j})^{\mathrm{H}}\boldsymbol{H}\boldsymbol{u}_{\mathrm{k}}\right\|^{2}), \tag{20}$$

where $\mathrm{m}_{jk}$ and $\Omega_{jk}$ represent the shape and expansion parameters of the Nakagami function, respectively.

## 2.3 Comparison of the Accuracy of Nakagami and Rayleigh Distributions

In order to verify Nakagami's accuracy in modeling the $\boldsymbol{O}$ matrix, we performed ray tracing simulations on a 7 × 7 × 3.5 $\mathrm{m}^3$ room using Feko+Winprop. The stereoscopic view of the room is shown in the Figure 1. There are varying numbers of glass windows on the left and right walls of the room, and a wooden door on the left wall. Around the room are a number of wooden tables and chairs, as well as some metal appliances. The transmitting antenna array, which is shown in the blue area of the Figure 1, is an 8 × 8 antenna array. They are evenly sampled in the room space every 0.5 m and set up a large number of receiving points to simulate. The transmitting and receiving antennas parameters are shown in the Table 1.

**Table 1.** *Parameters of the antennas.*

| central frequency | bandwidth | BS | | MS | |
|---|---|---|---|---|---|
| 4 GHz | 20 MHz | 8 × 8 array | | two whip antennas | |
| | | gain | 7 dBi | gain | 3 dBi |
| | | 3 dB angular width | -70 + 70 | direction | omni-directional |
| | | adjacent space | one wavelength | polarization | vertical polarized |

After obtaining the CIRs of 1176 sampling points, $\boldsymbol{O}$ can be obtained from (1) The shape and extension parameters of the Nakagami distribution can be obtained from (19) and (20), through which we can generate random elements that conform to Nakagami and Rayleigh distributions respectively. The Cumulative Distribution Functions (CDF) of elements follow Nakagami distribution, Rayleigh distribution, and simulation result are shown in Figure 2. Obviously that Nakagami distribution fits more closely, which verifies the third assumption.

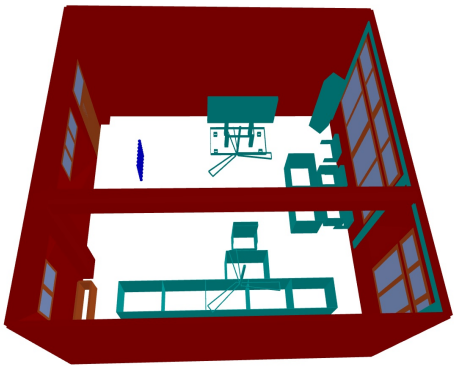

**Figure 1.** *3D diagram of room model for ray tracing simulations.*

## III. MASSIVE MIMO CHANNEL MEASUREMENT

### 3.1 Measurement Environment

We carried out these measurement activities in an $7 \times 7 \times 3$ m$^3$ indoor laboratory. Several tables and chairs, all made of wood, are placed in the laboratory. The tables lean against a 0.8 m high wall. In addition, multiple electronic devices are placed on these tables. Other objects such as air conditioners, whiteboards, and chairs are placed in the corners of the lab. The floor, walls, and ceiling are made of concrete, and

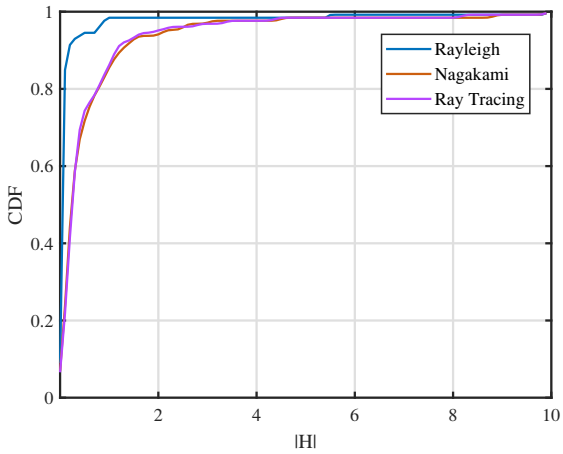


**Figure 2.** *CDFs of elements follow Nakagami distribution, Rayleigh distribution, and simulation result.*

the doors are made of glass. There are two windows on one side of the wall. The layout of the lab is shown in Figure 3.

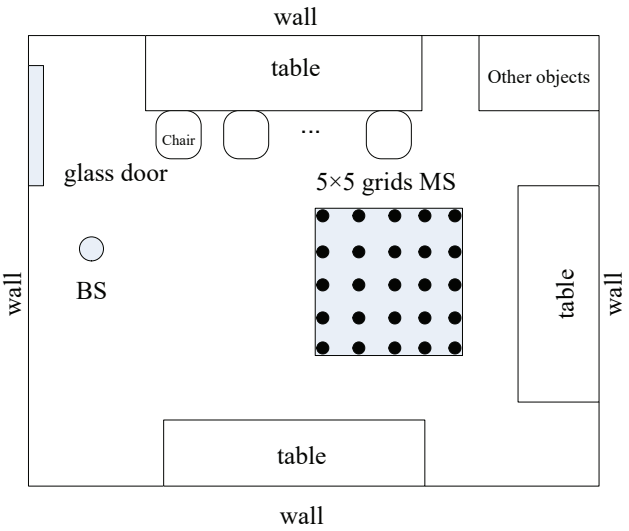


**Figure 3.** *Schematic diagram of measurement environments and setups.*

### 3.2 Measurement Environment

Based on USRP RIO software, developed by National Instruments [30, 35], we performed massive MIMO channel measurements by the LuMaLi test stand (shown in Figure 4). Via orthogonal frequency division multiplexing (OFDM) 4 GHz with 20 MHz bandwidth pilots are transmitted simultaneously at BS side. The real-time frequency response is then measured and stored through channel estimation at MS side. Use an identical reference clock to achieve frequency and phase synchronization. Use an oven-controlled crystal oscillator in a NI PXIe-6674T timing module to generate this clock. See [35] for a more detailed description of the LuMaLi test stand.

The BS is consisted with an 8 × 8 uniform planar array (the red area of the 8 × 16 array in Figure 4) and mount it upon a wooden frame 1.8 m high above the ground. Each element of the array is an omnidirectional monopole with a gain of 7 dBi and an angular width of -70 + 70 -3 dB on both the horizontal and vertical lines. Adjacent elements are spaced by a wavelength.

Two omni-directional vertically polarized whip antennas are used to simulate two users on the MS terminal. Each whip antenna operates at 3–6 GHz with a gain of 3 dBi.

The parameters of the measurement system are shown in Table 1.

BS is fixed at the north side of the laboratory, and its antenna position is shown in Figure 3. The measurements are made on a 5 × 5 grid with an interval of twice the wavelength per position, through which the small-scale fading can be studied. In order to test the far-field characteristics of massive MIMO channels, the MS position is selected so that the MS-BS distance is greater than the Rayleigh distance. First, the MS is located on one of the grids, and the MS receives a large number of fading signals from the MIMO channel. The MS moves to the next grid when the frequency response has been measured and saved, and the bench begins to measure the channel again. The MS antennas are aligned to the center of the BS array during the measurement.

The measured channel can be considered static during a channel snapshot.

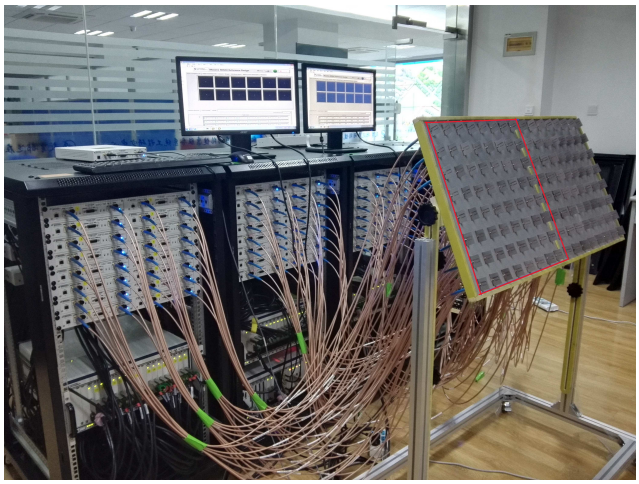

**Figure 4.** *Measurement system and BS antenna array.*

## IV. MASSIVE MIMO CHANNEL ANALYSIS OF CAPACITY, APS AND CHANNEL HARDENING

In massive MIMO systems, channel capacity and orthogonality are the most interesting indicators. This chapter mainly analyzes the relationship of channel capacity and orthogonal with $N_{\mathrm{MS}}$ and $N_{\mathrm{BS}}$ through simulation results.

### 4.1 Comparison with Other Models

Compare the proposed model with Kronecker model, Weichselberger model, and VCR in both accuracy and complexity to evaluate their performance.

By assuming the spatial covariance matrices to be spatially white, the unparameterized single-sided correlation matrices can be obtained as

$$\boldsymbol{R}_{\mathrm{MS}} = \mathrm{E}_{\boldsymbol{H}}(\boldsymbol{H}\boldsymbol{H}^{\mathrm{H}}), \tag{21}$$

and

$$\boldsymbol{R}_{\mathrm{BS}} = \mathrm{E}_{\boldsymbol{H}}(\boldsymbol{H}^{\mathrm{T}}\boldsymbol{H}^{*}). \tag{22}$$

The Kronecker model is expressed as

$$\boldsymbol{H}_{\mathrm{Kron}} = \frac{1}{P_{\boldsymbol{H}}}\boldsymbol{R}_{\mathrm{MS}}^{\frac{1}{2}}\boldsymbol{G}(\boldsymbol{R}_{\mathrm{BS}}^{\frac{1}{2}})^{\mathrm{T}}, \tag{23}$$

where $P_{\boldsymbol{H}} \triangleq E_{\boldsymbol{H}}\{\,\mathrm{tr}(\boldsymbol{H}\boldsymbol{H}^{\mathrm{H}})\,\}$ stands for the total mean energy of the channel. The entries of the matrix $\boldsymbol{G}$ are i.i.d. zero-mean complex-normal distributed [27].

The Weichselberger model is expressed as

$$\boldsymbol{H}_{\text{Weib}} = \boldsymbol{U}_{\text{MS}}(\boldsymbol{O}_{\text{weib}} \odot \boldsymbol{G})\boldsymbol{U}_{\text{BS}}^{\text{T}}, \tag{24}$$

where $\boldsymbol{U}_{\text{MS}}$ and $\boldsymbol{U}_{\text{BS}}$ are the eigenmatrices of $\boldsymbol{R}_{\text{MS}}$ and $\boldsymbol{R}_{\text{BS}}$, respectively. The $\boldsymbol{O}_{\text{Weib}}$ is the coupling matrix describing the average energy of eigenbases of BS and MS side. $\boldsymbol{G}$ is also an i.i.d. random matrix with zero-mean complex-normal distribution terms [29].

The VCR is expressed as

$$\boldsymbol{H}_{\text{VCR}} = \boldsymbol{A}_{\text{MS}}(\tilde{\boldsymbol{O}}_{\text{VCR}} \odot \boldsymbol{G})\boldsymbol{A}_{\text{BS}}, \tag{25}$$

where $\boldsymbol{A}_{\text{MS}}$ and $\boldsymbol{A}_{\text{BS}}$ are $\boldsymbol{N}_{\text{MS}} \times \boldsymbol{N}_{\text{MS}}$ and $\boldsymbol{N}_{\text{BS}} \times \boldsymbol{N}_{\text{BS}}$ channel independent discrete Fourier transform (DFT) matrices. $\boldsymbol{G}$ is still an i.i.d. random matrix with zero-mean complex-normal distribution terms. See [28] for more information about VCR.

The performances of the proposed model, the Weichselberger model, VCR, and Kronecker model are described in the this section. Firstly, model parameters are obtained from the measured data, and the CIRMs are obtained by Monte Carlo simulation. Then, the generated CIRM is compared with the measured results. The number of parameters and channel capacity are used as matrices to evaluate the complexity and accuracy of the proposed model.

The number of parameters required for these models are provided in Table 2. The Weichselberger model needs more parameters because it obtains the feature library at the BS end. Kronecker model needs a bit fewer parameters than Weichselberger model. In addition, the model requires two eigenvalue decomposition (EVD) operations. As the number of antennas increases, the Weichselberger model and Kronecker model will become more complex. It is worth noting that the complexity of the proposed approach to model CIRM is relatively low because the model omits the calculation of the eigenbases at the BS side. VCR has the least complexity among the four models, slightly lower than the proposed model. However the proposed model is more accurate than the VCR. To sum up, the proposed model provides better tradeoff between accuracy and complexity.

Compare the proposed model with Kronecker model, Weichselberger model, and VCR in both accuracy and complexity to evaluate their performance.

The performances of the proposed model, the Weichselberger model, VCR, and Kronecker model are described in the next section. Firstly, model parameters are obtained from the measured data, and the CIRMs are obtained by Monte Carlo simulation. Then, compared the generated CIRM with the measured results. The number of parameters and channel capacity are used as matrices to evaluate the complexity and accuracy of the proposed model.

Figure 5 shows the cumulative capacity distribution function for modeling and measurement. The signal-to-noise ratio is set as 10 dB. The results show that the proposed model is more consistent with the measured results than the Weichselberger model. Kolmogorov-Smirnov (K-S) test [36] is used for scientific quantitative fitting. This statistic is defined as

$$T_{\text{K-S}} = \sup_{x} \left| F_n(x) - F(x) \right|, \tag{26}$$

where sup $|\cdot|$ defines the upper bound of the set, while $F_n(x)$ and $F(x)$ are measured CDF and fitted CDF, respectively.

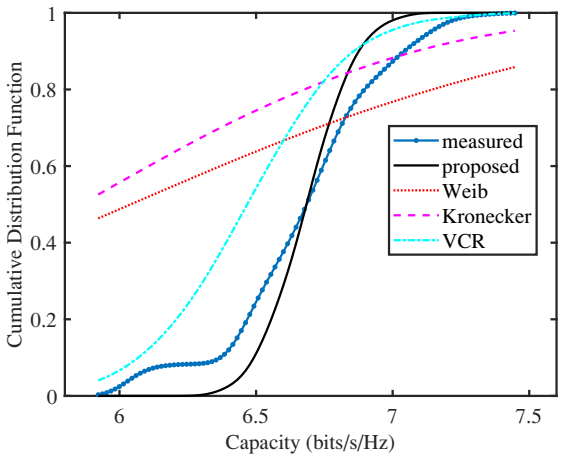


**Figure 5.** *Modeled and measured CDF of the capacity with SNR at 10 dB.*

In the K-S test, the smaller the statistic, the better the fitting. The fitting statistical value between the established model and the measured CDF is 0.11, while the result of Weichselberger model is 0.45. Therefore, it is clear that the proposed model is superior to Weichselberger model. This can be attributed to the fact that Nakagami distribution describes the attenuation property more accurately than Rayleigh distribution.

**Table 2.** *Number of the parameters and eigenvalue decomposition operations needed in different models.*

| model | proposed | Weib | Kron | VCR |
|---|---|---|---|---|
| number | $N_{\mathrm{BS}}N_{\mathrm{MS}}+N_{\mathrm{MS}}^2$ | $N_{\mathrm{BS}}N_{\mathrm{MS}}+N_{\mathrm{BS}}^2+N_{\mathrm{MS}}^2$ | $N_{\mathrm{BS}}^2+N_{\mathrm{MS}}^2$ | $N_{\mathrm{BS}}N_{\mathrm{MS}}$ |
| EVD | 1 | 2 | 2 | 0 |
| $N_{\mathrm{MS}}=2$, $N_{\mathrm{BS}}=64$ | 132 | 4228 | 4200 | 128 |
| $N_{\mathrm{MS}}=4$, $N_{\mathrm{BS}}=128$ | 518 | 16384 | 16400 | 512 |

## 4.2 Numerical Examples of APS

Figure 6 shows the 2-D joint APS for a single scenario. The measured spectrum (6c) shows a clear linkage of specific direction of departure(DoD) to specific direction of arrival(DoA). The Weichselberger model (6b) changes the spectrum slightly because assumption (4) in [29] is not completely fulfilled. However, the linkage of DoDs to DoAs is preserved to a large extent. Compared with the Weichselberger model, the proposed model (6a) differs greatly from the measurement results. But it's worth simplifying the complexity it brings.

The Bartlett spectrum utilizes the steering vectors at the MS side, $\boldsymbol{a}_{\mathrm{MS}}(\varphi_{\mathrm{MS}})$, and the BS side, $\boldsymbol{a}_{\mathrm{BS}}(\varphi_{\mathrm{BS}})$, to filter the MIMO channel. By extending Eq. (27) to the MIMO case, the Bartlett MIMO spectrum becomes

$$P_{BF}(\varphi_{\mathrm{RX}},\varphi_{\mathrm{TX}})=(\mathbf{a}_{\mathrm{RX}}(\varphi_{\mathrm{RX}})\otimes\mathbf{a}_{\mathrm{RX}}^{*}(\varphi_{\mathrm{RX}}))^{\mathrm{T}} *\mathbf{Q}_{\mathrm{H}}(\mathbf{a}_{\mathrm{TX}}(\varphi_{\mathrm{TX}})\otimes\mathbf{a}_{\mathrm{TX}}^{*}(\varphi_{\mathrm{TX}})). \tag{27}$$

In order to quantify the power spectrum differences, we use the Kullback-Leibler divergence(KLD) to describe the differences [37]. The KLD is defined as follows:

$$\gamma=\int_x\int_y\bar{P}_1(x,y)*\log\frac{\bar{P}_1(x,y)}{\bar{P}_2(x,y)}\mathrm{d}x\mathrm{d}y, \tag{28}$$

and

$$\bar{P}_i(x,y)=P_i(x,y)/\int_x\int_y P_i(x,y)\mathrm{d}x\mathrm{d}y, \tag{29}$$

where $\bar{P}_i(x,y)$ is the APS.

It can be seen in Table 3 that the KLDs of the proposed model are not much different from the Weib model. Define the variance rate as

$$dif=\frac{\gamma(\mathrm{proposed})-\gamma(\mathrm{Weib})}{\gamma(\mathrm{Weib})}. \tag{30}$$

**Table 3.** *KLDs of proposed model and Weib model.*

| SNR | 5dB | | 10dB | | 20dB | |
|---|---|---|---|---|---|---|
| $\gamma$(proposed) | 0.1037 | 0.0879 | 0.0574 | 0.0488 | 0.0150 | 0.0355 |
| $\gamma$(Weib) | 0.0915 | 0.0815 | 0.0552 | 0.0468 | 0.0145 | 0.0349 |

The difference rates at 5dB, 10dB, 20dB are 10.6%, 4.1%, 2.6%, respectivily. As the SNR increases, the difference rates decrease. Given the significant reduction in computational complexity brought about by the proposed model in massive MIMO, the cost of these accuracy is worth it.

## 4.3 Simulation Analysis of Channel Hardening

Channel hardening occurs when $N_{\mathrm{BS}}$ tends to be infinite in relation to the number of users ($N_{\mathrm{user}}$), the traversal capacity of each state converges to a certain value that is only related to large-scale fading. Channel hardening also refers to the fact that as antennas array grows, the non-diagonal elements of $\boldsymbol{H}^{\mathrm{H}}\boldsymbol{H}$ increase more slowly compared to the diagonal elements. For multi-user massive MIMO systems, user orthogonality is a measure of channel hardening characteristics. As $N_{\mathrm{BS}}$ of massive MIMO keeps increasing, the orthogonality of users becomes better and better. When $N_{\mathrm{BS}}$ tends to infinity, $\boldsymbol{H}^{\mathrm{H}}\boldsymbol{H}$ becomes a diagonal matrix. At this point, users are completely orthogonal without interfering with each other.

The joint orthogonality of users is considered from the downlink and is characterized by singular value spread of $\boldsymbol{H}$. Dispose $\boldsymbol{H}$ with singular value decom-

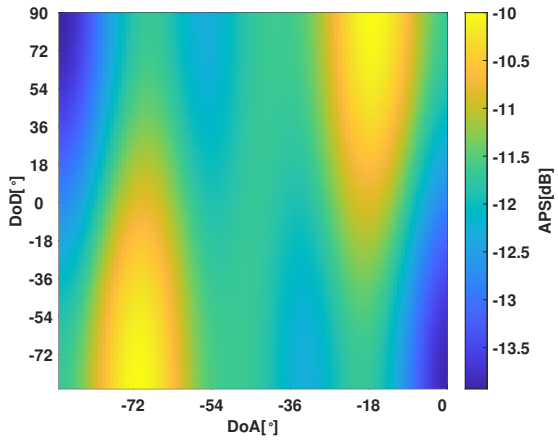


**(a)** *Weib model*

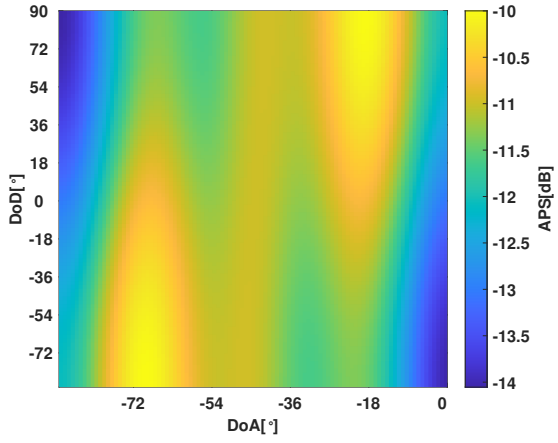


**(b)** *measured*

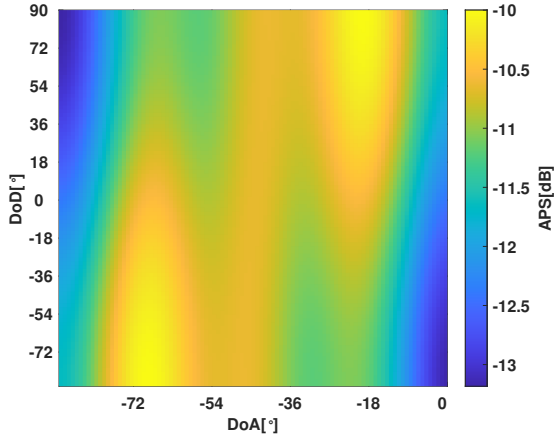


**(c)** *in an indoor scenario*

**Figure 6.** *APS of proposed model.*

position and get

$$\boldsymbol{H} = \boldsymbol{U}\boldsymbol{\Sigma}\boldsymbol{V}^{\mathrm{H}}, \tag{31}$$

where $\boldsymbol{H}$ is $N_{\mathrm{MS}} \times N_{\mathrm{BS}}$ channel matrix, $\boldsymbol{U}$ and $\boldsymbol{V}$ are unitary matrices, and $\boldsymbol{\Sigma}$ is $N_{\mathrm{MS}} \times N_{\mathrm{BS}}$ diagonal matrix. The diagonal elements ($\sigma_1$, $\sigma_2$, $\cdots$, $\sigma_k$) are singular values of $\boldsymbol{H}$ where $k$ denotes min ($N_{\mathrm{MS}}$, $N_{\mathrm{BS}}$). Singular value spread is defined as the ratio of the largest singular value to the smallest singular value

$$\mathrm{K} = \frac{\max\limits_{i} \sigma_i}{\min\limits_{i} \sigma_i}. \tag{32}$$

If singular value of $\boldsymbol{H}$ is very large, it indicates that there are at least two rows in $\boldsymbol{H}$ which are approximately parallel. That is to say there are at least two users whose vectors are nearly parallel and highly correlated. Singular value spread K = 1 when all users are completely independent and their vectors are strictly orthogonal.

Analyses of channel hardening with the help of typical coupling matrices that were introduced in [29]. Since $\boldsymbol{O}_1$, $\boldsymbol{O}_2$, and $\boldsymbol{O}_3$ are all singular matrices, their ranks are all equal to one and have only one singular value, which is not suitable for qualitative analysis by singular value spread.

For $\boldsymbol{O}_5$, as shown in Figure 7, when $N_{\mathrm{user}}$ = 2, with the increase of $N_{\mathrm{BS}}$, singular value spread CDF shifts to left gradually, indicating the orthogonality between users is more and more obvious, though which we can also become conscious of channel hardening process. It is also worth noting that when $N_{\mathrm{BS}}$ = 128, singular value spread distributed between 0 and 20 dB. The probability that the singular value spread is less than 10 dB is more than 70 percent, which denotes fine orthogonal property. Under the same circumstances, when $N_{\mathrm{BS}}$ is doubled, singular value spread decreases by about 5 dB. Similarly, when $N_{\mathrm{user}}$ = 8, singular value spread decreases gradually with the increase of $N_{\mathrm{BS}}$, and user orthogonality increase gradually. When $N_{\mathrm{BS}}$ = 128, singular value spread distributed between 90–120 dB. Though which we can still see channel hardening, but orthogonality is becoming increasingly difficult to maintain. When $N_{\mathrm{BS}}$ is doubled, singular value spread decreases by about 10–20 dB. For $N_{\mathrm{user}}$ = 128, increasing $N_{\mathrm{BS}}$ basically has no effect on reducing singular value spread. In addition, singular value spread rapidly rises to the minimum value of about 170 dB. Denoting the orthogonality between users is hard to be guaranteed, this is because as $N_{\mathrm{user}}$ grows, $N_{\mathrm{BS}}$ is

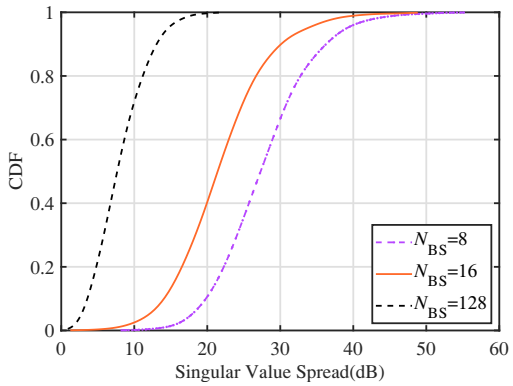


**(a)** $N_{\text{user}} = 2$

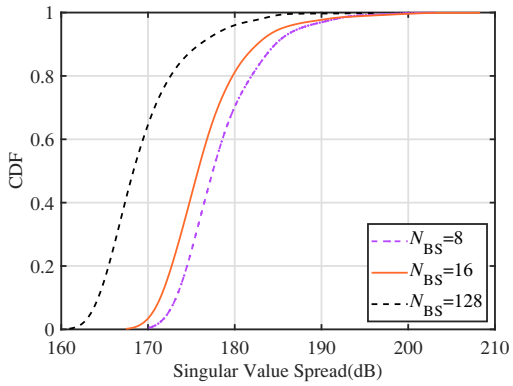


**(b)** $N_{\text{user}} = 16$

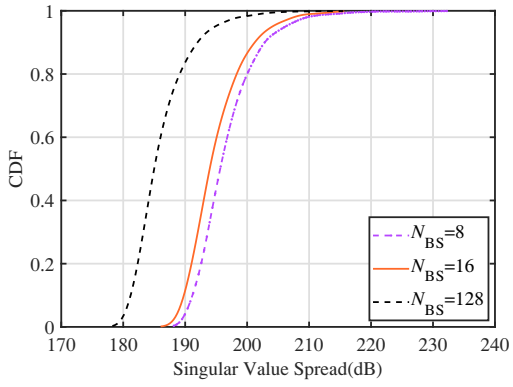


**(c)** $N_{\text{user}} = 128$

**Figure 7.** *Simulated singular value spread CDF of* $\boldsymbol{O}_4$ *under deferent* $N_{\text{user}}$ *and* $N_{\text{BS}}$ *at 10 dB.*

no longer meet the condition of being much larger than $N_{\text{user}}$. It is generally accepted that under rich scattering environment, $N_{\text{BS}}$ being ten times more than $N_{\text{user}}$, channel hardening can be manifested.

Channel hardening can also be characterized by the full correlation matrix, that is, when the antenna array increases, the non-diagonal elements of the $\boldsymbol{H}^{\text{H}}\boldsymbol{H}$ increase very slowly compared with the diagonal elements. Based on this, we conducted further simulation analysis, as shown in Figure 8, when $N_{\text{MS}}$ is fixed and $N_{\text{BS}}$ increases from 256 to 1024, the non-diagonal elements of $\boldsymbol{H}^{\text{H}}\boldsymbol{H}$ approach zero, while the diagonal elements approach $N_{\text{MS}}$ as 2. Similarly, as shown in Figure 9, when $N_{\text{MS}}$ remains unchanged at 32 and $N_{\text{BS}}$ increases from 256 to 1024, the non-diagonal elements of $\boldsymbol{H}^{\text{H}}\boldsymbol{H}$ approach zero, while the diagonal elements approach to $N_{\text{MS}}$, in this example, 32. Contrast Figure 8 and Figure 9 one can come to a conclusion that increasing $N_{\text{MS}}$ affects only the absolute value of $\boldsymbol{H}^{\text{H}}\boldsymbol{H}$ but not the relative value. This means that changing the number of $N_{\text{MS}}$ has no significant effect on channel hardening while in fact, it should. It is the accuracy sacrifice of this model to reduce complexity. However, considering the reality of MIMO, that is, $N_{\text{MS}}$ is still small compared to $N_{\text{BS}}$, this sacrifice is worth it. At the same time, this also causes that the model can only show obvious channel hardening when $N_{\text{BS}}$ is large enough. Therefore, this model is more suitable for the situation that $N_{\text{BS}}$ is large enough than $N_{\text{MS}}$ in the future massive MIMO construction. It is worth noting that Figure 8 have sub-diagonal peak phenomenon, which is an inevitable phenomenon based on the virtual channel representation model. This is consistent with the result in [29].

## V. CONCLUSION

In this paper, a novel CIRM model for massive MIMO channel by combining the advantages of VCR and Weichselberger model has been proposed. This CIRM can be expressed as a sum of couplings between the steering vectors at BS side and eigenbases at MS side. Steering vectors can be seemed as eigenbases at BS side as long as the array size is large enough to provide high spatial resolution. The fading properties of the couplings between the steering vectors and the eigenbases have been destribed with Nakagami distribution. The accuracy of the Nakagami distribution has been verified by Feko+Winprop ray tracing. The accuracy of this model has been proved through comparison of channel capacities with some classic models. Finally, the simulation analysis of the channel hardening characteristics have been carried out.

The proposed model can be employed for the link level simulation and the interference alignment in future massive MIMO communication system.

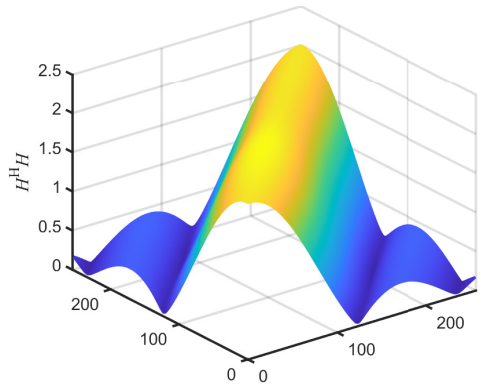


**(a)** $N_{\mathrm{MS}} = 2$, $N_{\mathrm{BS}} = 256$

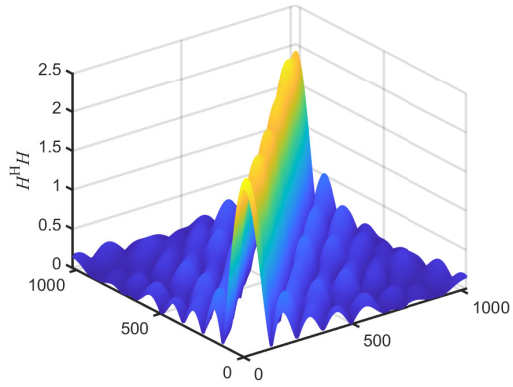


**(b)** $N_{\mathrm{MS}} = 2$, $N_{\mathrm{BS}} = 1024$

**Figure 8.** *Simulated elements of* $\boldsymbol{H}^{\mathrm{H}}\boldsymbol{H}$.

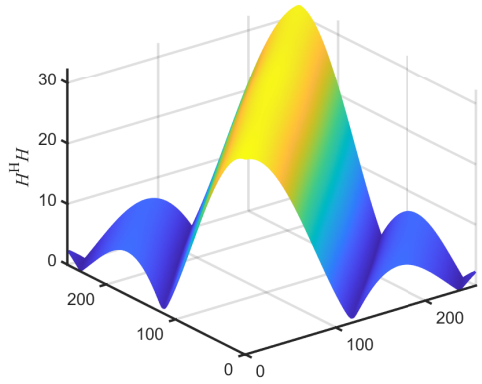


**(a)** $N_{\mathrm{MS}} = 32$, $N_{\mathrm{BS}} = 256$

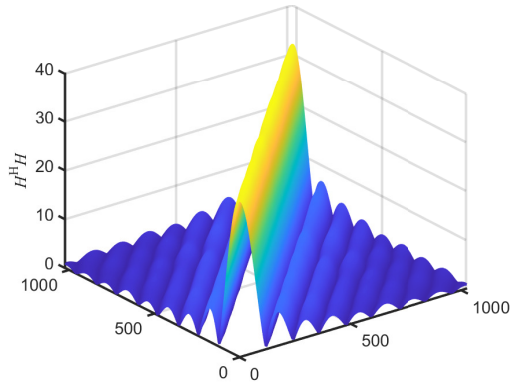


**(b)** $N_{\mathrm{MS}} = 32$, $N_{\mathrm{BS}} = 1024$

**Figure 9.** *Simulated elements of* $\boldsymbol{H}^{\mathrm{H}}\boldsymbol{H}$.

## ACKNOWLEDGEMENT

This work was supported by the Key R&D Project of Jiangsu Province (Modern Agriculture) under Grant BE2022322 the "PilotPlan" Internet of Things special project (China Institute of IoT (wuxi) and Wuxi Internet of Things Innovation Promotion Center) under Grant 2022SP-T16-B,in part by the 111 Project under Grant B12018, in part by the Six talent peaks project in Jiangsu Province, in part by the open foundation of Key Laboratory of Wireless Sensor Network and Communication, Shanghai Institute of Microsystem and Information Technology, Chinese Academy of Sciences under Grant 20190917, and in part by the open research fund of Key Lab of Broadband Wireless Communication and Sensor Network Technology (Nanjing University of Posts and Telecommunications, Ministry of Education). (*Corresponding author: Chengxiang Wang*.)

## References

[1] X. You, C. Wang, *et al.*, "Towards 6g wireless communication networks: Vision, enabling technologies, and new paradigm shifts," *Science China Information Sciences*, 2021, vol. 64, pp. 1–74.

[2] S. Chen, Y. Liang, *et al.*, "Vision, requirements, and technology trend of 6g: How to tackle the challenges of system coverage, capacity, user data-rate and movement speed," *IEEE Wireless Communications*, 2020, vol. 27, no. 2, pp. 218–228.

[3] Z. Zhang, Y. Xiao, *et al.*, "6g wireless networks: Vision, requirements, architecture, and key technologies," *IEEE Vehicular Technology Magazine*, 2019, vol. 14, no. 3, pp. 28–41.

[4] W. Saad, M. Bennis, *et al.*, "A vision of 6g wireless systems: Applications, trends, technologies, and open research problems," *IEEE Network*, 2019, vol. 34, no. 3, pp. 134–142.

[5] J. Zhang, Z. Zheng, *et al.*, "3d mimo for 5g nr: Several observations from 32 to massive 256 antennas based on channel measurement," *IEEE Communications Magazine*, 2018, vol. 56, no. 3, pp. 62–70.

[6] Y. Tan, C. Wang, *et al.*, "A novel b5g frequency nonstationary wireless channel model," *IEEE Transactions on Antennas and Propagation*, 2021, vol. 69, no. 8, pp. 4846–4860.

[7] J. Zhang, P. Tang, *et al.*, "Channel measurements and models for 6g: current status and future outlook," *Frontiers of*

*Information Technology & Electronic Engineering*, 2020, vol. 21, no. 1, pp. 39–61.

[8] T. Jiang, J. Zhang, *et al.*, "3gpp standardized 5g channel model for iiot scenarios: A survey," *IEEE Internet of Things Journal*, 2021, vol. 8, no. 11, pp. 8799–8815.

[9] S. Wu, C. Wang, *et al.*, "A general 3-d non-stationary 5g wireless channel model," *IEEE Transactions on Communications*, 2017, vol. 66, no. 7, pp. 3065–3078.

[10] J. Wang, C. Wang, *et al.*, "A general 3d space-time-frequency non-stationary thz channel model for 6g ultra-massive mimo wireless communication systems," *IEEE Journal on Selected Areas in Communications*, 2021, vol. 39, no. 6, pp. 1576–1589.

[11] J. Bian, C. Wang, *et al.*, "A general 3d non-stationary wireless channel model for 5g and beyond," *IEEE Transactions on Wireless Communications*, 2021, vol. 20, no. 5, pp. 3211–3224.

[12] W. C. Lee, *Mobile Communications Engineering: Theory and Applications*. McGraw-Hill, Inc., 1997.

[13] G. Yue, D. Yu, *et al.*, "Measurements and ray tracing simulations for non-line-of-sight millimeter-wave channels in a confined corridor environment," *IEEE Access*, 2019, vol. 7, pp. 85 066–85 081.

[14] J. Huang, C. Wang, *et al.*, "Multi-frequency mmwave massive mimo channel measurements and characterization for 5g wireless communication systems," *IEEE Journal on Selected Areas in Communications*, 2017, vol. 35, no. 7, pp. 1591–1605.

[15] V. A. Fono, L. Talbi, *et al.*, "Deterministic modeling of indoor stairwells propagation channel," *IEEE Antennas and Wireless Propagation Letters*, 2019, vol. 19, no. 2, pp. 327–331.

[16] F. Sheikh, Y. Gao, *et al.*, "A study of diffuse scattering in massive mimo channels at terahertz frequencies," *IEEE Transactions on Antennas and Propagation*, 2019, vol. 68, no. 2, pp. 997–1008.

[17] M. Raspopoulos, "Multidevice map-constrained fingerprint-based indoor positioning using 3-d ray tracing," *IEEE Transactions on Instrumentation and Measurement*, 2017, vol. 67, no. 2, pp. 466–476.

[18] P. Petrus, J. H. Reed, *et al.*, "Geometrical-based statistical macrocell channel model for mobile environments," *IEEE Transactions on Communications*, 2002, vol. 50, no. 3, pp. 495–502.

[19] M. Zhang, P. J. Smith, *et al.*, "An extended one-ring mimo channel model," *IEEE Transactions on Wireless Communications*, 2007, vol. 6, no. 8, pp. 2759–2764.

[20] *Preliminary Draft New Report ITU-R M. [IMT-2020.EVAL], Channel Model (Part), Version 1*, document ITU-R R15-WP5D-170613-TD-0332, 2017.

[21] Q. Zhu, C. Wang, *et al.*, "3gpp tr 38.901 channel model," *Wiley 5G Ref: The Essential 5G Reference Online*, 2019, pp. 1–35.

[22] L. Liu, C. Oestges, *et al.*, "The cost 2100 mimo channel model," *IEEE Wireless Communications*, 2012, vol. 19, no. 6, pp. 92–99.

[23] S. Jaeckel, L. Raschkowski, *et al.*, "Quasi deterministic radio channel generator user manual and documentation (v2. 2.0)," *Tech. Rep*, 2019.

[24] Y. Zhang, L. Pang, *et al.*, "3-d mimo parametric stochastic channel model for urban macrocell scenario," *IEEE Transactions on Wireless Communications*, 2017, vol. 16, no. 7, pp. 4246–4260.

[25] J. Chen, X. Yin, *et al.*, "Measurement-based massive mimo channel modeling for outdoor los and nlos environments," *IEEE Access*, 2017, vol. 5, pp. 2126–2140.

[26] R. Zhang, X. Lu, *et al.*, "Measurement and modeling of angular spreads of three-dimensional urban street radio channels," *IEEE Transactions on Vehicular Technology*, 2016, vol. 66, no. 5, pp. 3555–3570.

[27] J. Kermoal, L. Schumacher, *et al.*, "A stochastic mimo radio channel model with experimental validation," *IEEE Journal on Selected Areas in Communications*, 2002, vol. 20, no. 6, pp. 1211–1226.

[28] A. M. Sayeed, "Deconstructing multiantenna fading channels," *IEEE Transactions on Signal Processing*, 2002, vol. 50, no. 10, pp. 2563–2579.

[29] W. Weichselberger, M. Herdin, *et al.*, "A stochastic mimo channel model with joint correlation of both link ends," *IEEE Transactions on Wireless Communications*, 2006, vol. 5, no. 1, pp. 90–100.

[30] Y. Yu, P. Cui, *et al.*, "Measurement and empirical modeling of massive mimo channel matrix in real indoor environment," in *2016 8th International Conference on Wireless Communications & Signal Processing (WCSP)*. IEEE, 2016, pp. 1–5.

[31] M. Eriksson and T. Olofsson, "On long-term statistical dependences in channel gains for fixed wireless links in factories," *IEEE Transactions on Communications*, 2016, vol. 64, no. 7, pp. 3078–3091.

[32] X. Gao, O. Edfors, *et al.*, "Antenna selection in measured massive mimo channels using convex optimization," in *2013 IEEE Globecom Workshops (GC Wkshps)*. IEEE, 2013, pp. 129–134.

[33] X. Gao, O. Edfors, *et al.*, "Massive mimo performance evaluation based on measured propagation data," *IEEE Transactions on Wireless Communications*, 2015, vol. 14, no. 7, pp. 3899–3911.

[34] A. O. Martinez, E. De Carvalho, *et al.*, "Towards very large aperture massive mimo: A measurement based study," in *2014 IEEE Globecom Workshops (GC Wkshps)*, 2014, pp. 281–286.

[35] J. Vieira, S. Malkowsky, *et al.*, "A flexible 100-antenna testbed for massive mimo," in *2014 IEEE Globecom Workshops (GC Wkshps)*, 2014, pp. 287–293.

[36] F. J. Massey Jr, "The kolmogorov-smirnov test for goodness of fit," *Journal of the American Statistical Association*, 1951, vol. 46, no. 253, pp. 68–78.

[37] T. T. Georgiou, "Distances and riemannian metrics for spectral density functions," *IEEE Transactions on Signal Processing*, 2007, vol. 55, no. 8, pp. 3995–4003.

## Biographies

***Yang Liu*** was born in Wuxi, Jiangsu Province, China, in 1988. He received the Ph.D. degree in communication and information system from Key Laboratory of Wireless Communication, Nanjing University of Posts and Telecommunications (NUPT), Nanjing, China, in 2016. He is currently an associate Professor in Institute of IOT Engineering, Jiangnan University, Wuxi, Jiangsu Province. He has authored and co-authored over 10 technical papers published in peer-reviewed international journals and conference proceedings. His research interests include the wireless channel modeling and network coding.

***Gang Li*** was born in Yantai, Shandong Province, China, in 1998. He graduated from Institute of IOT Engineering, Jiangnan University, Wuxi, Jiangsu Province, China, in 2020. He is currently pursuing a master's degree in Institute of IOT Engineering, Jiangnan University, Wuxi, Jiangsu Province. His research interests include wireless propagation and wireless channel modeling.

***Chengxiang Wang*** received the BSc and MEng degrees in Communication and Information Systems from Shandong University, China, in 1997 and 2000, respectively, and the PhD degree in Wireless Communications from Aalborg University, Denmark, in 2004.

He was a Research Assistant with the Hamburg University of Technology, Hamburg, Germany, from 2000 to 2001, a Visiting Researcher with Siemens AG Mobile Phones, Munich, Germany, in 2004, and a Research Fellow with the University of Agder, Grimstad, Norway, from 2001 to 2005. He has been with Heriot-Watt University, Edinburgh, U.K., since 2005, where he was promoted to a Professor in 2011. In 2018, he joined the National Mobile Communications Research Laboratory, Southeast University, China, as a Professor. He is also a part-time professor with the Purple Mountain Laboratories, Nanjing, China. He has authored four books, three book chapter, and more than 530 papers in refereed journals and conference proceedings, including 27 ESI Highly Cited Papers. He has also delivered 27 Invited Keynote Speeches/Talks and 18 Tutorials in international conferences. His current research interests include wireless channel measurements and modeling, B5G wireless communication networks, and applying artificial intelligence to wireless networks. Prof. Wang is a Member of the Academia Europaea (The Academy of Europe), a fellow of the IET, an IEEE Communications Society Distinguished Lecturer in 2019 and 2020, and a Highly-Cited Researcher recognized by Clarivate Analytics in 2017-2020. He is currently an Executive Editorial Committee member for the *IEEE Transactions on Wireless Communications*. He has served as an Editor for nine international journals, including the *IEEE Transactions on Wireless Communications* from 2007 to 2009, the *IEEE Transactions on Vehicular Technology* from 2011 to 2017, and the *IEEE Transactions on Communications* from 2015 to 2017. He was a Guest Editor for the *IEEE Journal on Selected Areas in Communications*, Special Issue on Vehicular Communications and Networks (Lead Guest Editor), Special Issue on Spectrum and Energy Efficient Design of Wireless Communication Networks, and Special Issue on Airborne Communication Networks. He was also a Guest Editor for the *IEEE Transactions on Big Data*, Special Issue on Wireless Big Data, and is a Guest Editor for the *IEEE Transactions on Cognitive Communications and Networking*, Special Issue on Intelligent Resource Management for 5G and Beyond. He received twelve Best Paper Awards from IEEE GLOBECOM 2010, IEEE ICCT 2011, ITST 2012, IEEE VTC 2013.